Experimental Twin-Field Quantum Key Distribution over 1000 km Fiber Distance

Yang Liu,[1,2,3] Wei-Jun Zhang,[4] Cong Jiang,[2,3] Jiu-Peng Chen,[1,2] Chi Zhang,[1,2] Wen-Xin Pan,[1] Di Ma,[2] Hao Dong,[1,2] Jia-Min Xiong,[4] Cheng-Jun Zhang,[5] Hao Li,[4] Rui-Chun Wang,[6] Jun Wu,[6] Teng-Yun Chen,[1,3] Lixing You,[4,*] Xiang-Bin Wang,[2,3,7,†] Qiang Zhang,[1,2,3,‡] and Jian-Wei Pan[1,3,¶]

[1]*Hefei National Research Center for Physical Sciences at the Microscale and School of Physical Sciences, University of Science and Technology of China, Hefei 230026, China*

[2]*Jinan Institute of Quantum Technology and CAS Center for Excellence in Quantum Information and Quantum Physics, University of Science and Technology of China, Jinan 250101, China*

[3]*Hefei National Laboratory, University of Science and Technology of China, Hefei 230088, China*

[4]*State Key Laboratory of Functional Materials for Informatics, Shanghai Institute of Microsystem and Information Technology, Chinese Academy of Sciences, Shanghai 200050, China*

[5]*Photon Technology (Zhejiang) Co. Ltd., Jiaxing 314100, China*

[6]*State Key Laboratory of Optical Fibre and Cable Manufacture Technology, Yangtze Optical Fibre and Cable Joint Stock Limited Company, Wuhan 430073, China*

[7]*State Key Laboratory of Low Dimensional Quantum Physics, Department of Physics, Tsinghua University, Beijing 100084, China*

(Received 3 February 2023; accepted 10 April 2023; published 25 May 2023)

Quantum key distribution (QKD) aims to generate secure private keys shared by two remote parties. With its security being protected by principles of quantum mechanics, some technology challenges remain towards practical application of QKD. The major one is the distance limit, which is caused by the fact that a quantum signal cannot be amplified while the channel loss is exponential with the distance for photon transmission in optical fiber. Here using the 3-intensity sending-or-not-sending protocol with the actively-odd-parity-pairing method, we demonstrate a fiber-based twin-field QKD over 1002 km. In our experiment, we developed a dual-band phase estimation and ultra-low noise superconducting nanowire single-photon detectors to suppress the system noise to around 0.02 Hz. The secure key rate is 9.53×10^{-12} per pulse through 1002 km fiber in the asymptotic regime, and 8.75×10^{-12} per pulse at 952 km considering the finite size effect. Our work constitutes a critical step towards the future large-scale quantum network.

DOI: 10.1103/PhysRevLett.130.210801

Introduction.—With the security protected by laws of quantum mechanics, quantum key distribution (QKD) [1–7] can distribute secret private keys between remote parties through photon transmission. Given the advantage in security, there are also some barriers to the practical application of QKD. The biggest challenge is the channel loss to the single-photon level weak light used in QKD. This limits the secure distance of practical QKD severely since a quantum signal cannot be perfectly cloned [8]. The channel transmittance decreases exponentially with the distance, hence the channel and detection noise prevents the QKD system to produce secure key in a long distance. Moreover, with the number of heralded events being smaller in longer distance QKD, the finite-key effect becomes a problem that reduces the generation of key bits. Through the extensive studies of QKD in the past decades, much progress has been made towards practical applications. Alongside these studies, the secure distance has been raised drastically with several notable breakthroughs in both theory and technology, especially after the twin-field QKD (TF-QKD) is proposed [9].

The key rate of traditional QKD protocols scales linearly with the channel transmittance η. TF-QKD [9] improves this relation to $\sqrt{\eta}$ without using a quantum memory or trusted relay. This provides a promising way to a longer secure distance of point-to-point QKD and to a large-scale quantum network with fewer trusted relays. So far, TF-QKD has been demonstrated experimentally in lab [10–20] through up to 830-km spooled fiber [20], and in the field test through 511-km deployed fiber between metropolitans [17].

Here we demonstrate a TF-QKD using sending-or-not-sending (SNS) protocol [21] over long distance fiber spools. The advanced 3-intensity decoy-state method [22] and the actively-odd-parity-pairing (AOPP) [23,24] are used to improve the key rate. The system noise is suppressed in experiment using narrow filter assisted superconducting nanowire single-photon detectors (SNSPDs) and using a data postprocessing based dual-band phase estimation method. We achieve a 1002 km distribution distance in the asymptotic regime, and a 952 km distribution distance

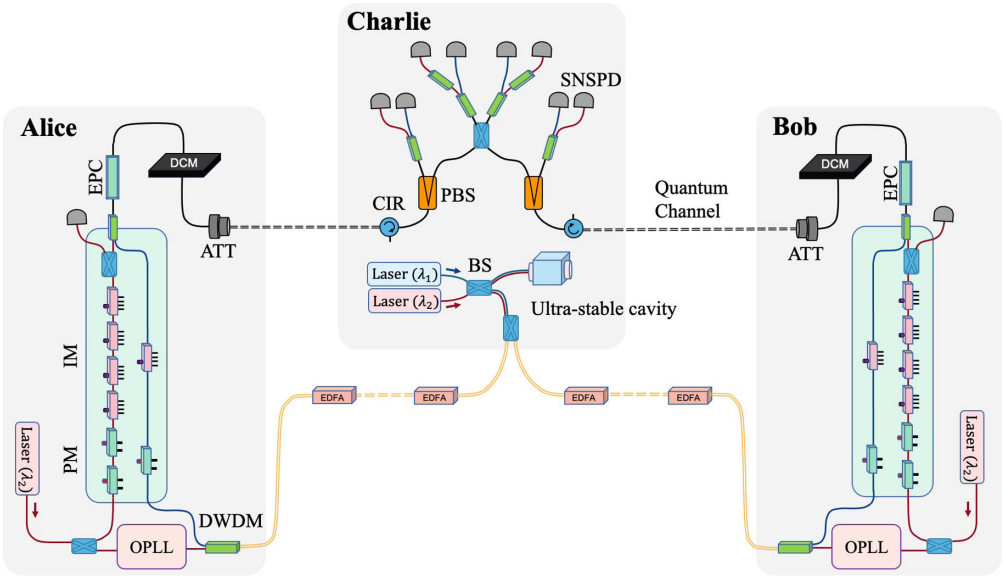

FIG. 1. Experimental setup. In Charlie's station, two lasers ($\lambda_1 = 1548.51$ and $\lambda_2 = 1550.12$ nm) are frequency locked to an ultrastable cavity, then combined, and distributed to Alice (Bob) via 450 (450 km) single mode fiber spools. In Alice's (Bob's) station, λ_2 is regenerated with an optical phase-locked loop (OPLL). The λ_2 light is encoded to dim phase reference and quantum signal with time multiplexing, then combined with the λ_1 strong phase reference with wavelength multiplexing. Signals from Alice and Bob are transmitted to Charlie for interference. The interference results are measured with SNSPDs. Additional SNSPDs are used to monitor the signal intensities at Alice and Bob, the polarization and the relative delay at Charlie. Beam splitter (BS); polarization beam splitters (PBS); intensity modulator (IM), phase modulator (PM); attenuator (ATT); dense wavelength division multiplexing (DWDM); optical circulator (CIR); erbium-doped fibre amplifier (EDFA); dispersion compensation module (DCM); electronic polarization controller (EPC).

considering the finite size effect. Further, a 47.06 kbps secure key rate is achieved through 202 km fibers.

Protocol.—We adopt the SNS protocol [21] using 3 intensities (3-intensity SNS-TF-QKD) and the improved key rate calculation [22]. We also apply the AOPP [23] method to reduce the bit-flip error rate. Different from [25,26], we use the advanced decoy-state analysis [22] to improve the secure key rate. Say, Alice takes decoy-state analysis after bit-flip error correction. This means we can use the whole numbers of heralded time windows of each intensity for the decoy-state analysis [22]. This improves the key rate because on the one hand, we don't need to spend a subset of code bits only for decoy-state analysis, on the other hand, we have a larger data size in the decoy-state analysis and hence the finite-data effect is reduced. There are three weak coherent state sources from Alice and Bob: the vacuum source v, the decoy source x, and the signal source y whose intensities are $\mu_v = 0, \mu_x, \mu_y$, respectively. In each time window, Alice (Bob) randomly chooses one source l (r) from the three candidate sources with probability p_l (p_r) with $l, r = v, x, y$ and then sends the prepared pulse to the measurement station which is controlled by Charlie. Charlie is assumed to measure the interference result of the incoming pulse pair and announce the measurement results to Alice and Bob. In the protocol, Alice and Bob send N pulse pairs to Charlie, then Charlie announces those time windows with correct heralding. Finally, they distill the secure keys according to the following formula:

$$R = \frac{1}{N}\{n_1'[1 - H(e_1'^{\mathrm{ph}})] - f n_t' H(E_t')\}, \tag{1}$$

where R is the key rate of per sending-out pulse pair; n_1' is the lower bound of the number of survived untagged bits after AOPP and $e_1'^{\mathrm{ph}}$ is the upper bound of the phase-flip error rate of those survived untagged bits after AOPP; n_t' is the number of survived bits after AOPP and E_t' is the corresponding bit-flip error rate in those survived bits; f is the error correction inefficiency which we set to $f = 1.16$; $H(x) = -x\log_2 x - (1-x)\log_2(1-x)$ is the Shannon entropy. To consider finite-key effects, they need to estimate parameters n_1' and $e_1'^{\mathrm{ph}}$ faithfully with finite data, also, tailing terms [22] have to be added to Eq. (1) [22,24,27]. (See Supplemental Material [28] for details of the theoretical calculations, which includes Refs. [29,30].)

Experiment.—The experimental setup is shown in Fig. 1. Two lasers with wavelengths λ_1 (1548.51 nm) and λ_2 (1550.12 nm) are frequency locked to an ultrastable cavity at Charlie, using the Pound-Drever-Hall (PDH) technique [31–33]. The Hertz level linewidth light is then sent to Alice and Bob.

Alice and Bob modulate the λ_1 light from Charlie to a 400 ns pulse in each 1 μs period, as the "strong phase reference." A locally prepared laser with a nominal linewidth of 1 kHz is locked to the λ_2 light from Charlie using an optical phase-locked loop (OPLL). This λ_2 light is modulated with a 100 ms period. The initial 40 ms of light serves as the "dim phase reference," with intensity set to a higher level for phase estimation at Charlie; the remaining 60 ms is used as "quantum signals," with intensity set to the single photon level. Four different relative phases between Alice and Bob ($\delta_{AB} = \{0, \pi/2, \pi, 3\pi/2\}$) are modulated for both the strong phase reference and dim phase reference.

The quantum signals are modulated to 3 intensities and 16 phases, following the 3-intensity SNS-TF-QKD protocol. A fraction of the λ_2 light is monitored to stabilize the intensities of the decoy states and the dim phase reference, before attenuating to a single photon level. Then, the λ_1 and λ_2 light are combined and transmitted to Charlie through ultra-low-loss fibers with an average attenuation of less than 0.157 dB/km.

At Charlie's measurement station, one output of the PBS is used to monitor the light from Alice and Bob. The polarization is adjusted according to the detection rate at this monitoring port. The λ_1 detections is set between 75 kHz and 300 kHz, and the λ_2 as low as possible. The rising edges of the λ_1 pulses are used to compensate the relative delay between Alice's and Bob's signals (See Supplemental Material [28] for details of the feedback system). The light from the signal ports of the PBSs are combined for interference. The interference output of the λ_1 and λ_2 light are separated and filtered by DWDMs, measured with SNSPDs, and recorded with a Time Tagger.

The most challenging barriers to achieving ultralong distance TF-QKD lies in reducing the channel loss and the system noise. To reduce channel loss, we adopted the "pure silica core" technology by reducing the doped Ge in the core, and we decreased the fictive temperature in the manufacturing process. We adopted a large effective area design with around 125 μm^2 effective area, to reduce the nonlinear effect in transmission. To reduce the system noise, we adopted low temperature filters in the SNSPDs resulting a lower dark count rate (DCR); we developed a time-multiplexing dual-band phase estimation method that helps to control spurious photons from the channel.

The main contribution of the dark count noise of the NbN SNSPDs is the blackbody radiation coming along the input fiber. This noise is reduced using multiple filters. The long-wavelength (> 2 μm) noise photons are filtered by coiling the fiber to a 28 mm diameter at 40 K cold plate. Other blackbody photons are filtered out by inserting a customized cryogenic bandpass filter (BPF) before coupling the fiber to the SNSPD chip at 2.2 K cold plate [34]. The BPF is centered at 1550 nm with a 5 nm bandwidth and a 85% transmittance. After suppressing the blackbody photons, the DCR is reduced from about 10 Hz to about 0.02 Hz. Further, the photon absorption is optimized by using a distributed Bragg reflector (DBR) based optical cavity [35] to enhance the detection efficiency to $94 \pm 2\%$. We note the system detection efficiency decreases to around 60% due to the loss in transmitting and insertion loss of the BPF.

The dominant source of noises from the channel is identified as the re-Rayleigh scattering of the phase estimation signal in pervious studies [15,17]. For example, approximately 8 Hz re-Rayleigh scattering is expected when the detected rate of the time-multiplexed phase reference is 2 MHz [15,17]. The dual-band stabilization method reduces the re-Rayleigh scattering noise by setting the wavelength of the phase reference light different from the quantum signal [19]. The re-Rayleigh scattering generated by the λ_1 strong phase reference can be easily filtered with a DWDM. After compensating the fast phase fluctuation with λ_1, the residual phase of the λ_2 quantum signal can be corrected with a much weaker dim phase reference time multiplexed with the quantum signal.

However, in the ultralong fiber scenario, the noise induced by the λ_1 strong phase reference cannot be neglected. The measured noises in the λ_2 channel reach approximately 0.55 Hz when the detected reference count is 2 MHz through a 300 km fiber. As a comparison, the crosstalk noise to the λ_2 channel is around 10^{-3} Hz when removing the fiber spools and setting the same λ_1 detection rate. We attribute the main source of noise to the spontaneous Raman scattering of the λ_1 light as it propagates through the fiber. (See Supplemental Material [28] for details of the measurement of noises).

To avoid the spontaneous Raman scattering noise, we modulate the strong phase reference to a 400 ns pulse in the 1 μs period. The quantum signals is transmitted solely during the last 600 ns when λ_1 is set to vacuum. The noise in the signal period is filtered with time division.

We developed data postprocessing methods for the time-multiplexed dual-band phase estimation that removes the need of active phase modulators and real-time feedback circuits for phase compensation.

The first step is to estimate the relative phase of λ_1 strong phase reference. We follow the procedure in our previous phase estimation method [12] to correct fast phase changes. As shown in Fig. 2 and its inset (a), the phase drift of the strong phase reference shows a monodirectional drift in a large timescale, while fast oscillations appears in short period.

The second step is to estimate the phase of the quantum signal. The simplest method is to set the strong phase reference directly as the estimation of the phase of quantum signal:

$$\phi_s(t) = \phi_r(t) + \phi_s(0) - \phi_r(0). \tag{2}$$

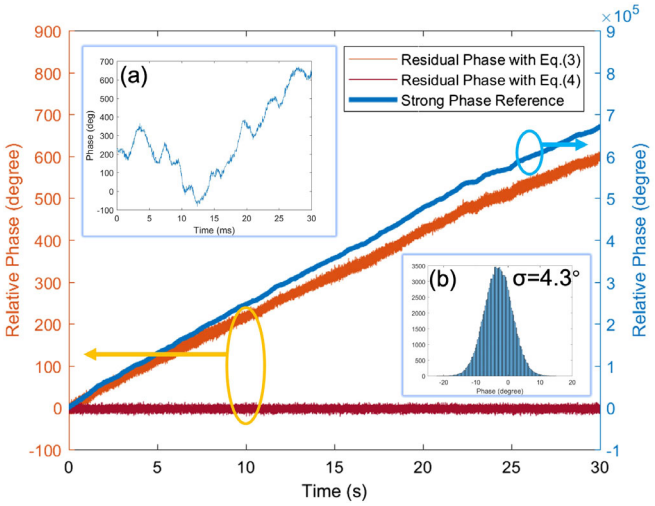

FIG. 2. Dual-band stabilization with data postprocessing. Main figure: blue, free phase drift estimated with strong phase reference in 30 s period; orange, residual phase drift after simple compensation with Eq. (2); red, residual phase drift after fine compensation with Eq. (4). Inset (a) the first 30 ms of the free phase drift, and (b) histogram of the residual phase with fine compensation (red line in main figure).

We define the residual phase ϕ_{residual} as the difference between the estimated phase $\phi_s(t)$ and the actual phase $\phi_{\text{s\_act}}(t)$ of the quantum signal:

$$\phi_{\text{residual}}(t) = \phi_{\text{s\_act}}(t) - \phi_s(t) \tag{3}$$

The residual phase ϕ_{residual} stands for the error induced in the phase estimation process, which will affect the QBER in the X basis. A smaller residual phase indicates a better estimation.

With the simple estimation method, the residual phase is already reduced by more than 1000 times compared with free drift, similar to the reported hardware-based dual-band compensation [18]. The residual phase in Eq. (2) is mainly contributed by the wavelength difference. It is possible to take this effect into consideration in data processing:

$$\phi_s(t) = \phi_r(t) \times \lambda_2/\lambda_1 + \phi_s(0) - \phi_r(0). \tag{4}$$

Taking the wavelength difference into consideration by Eq. (4), the residual phase is further suppressed, resulting in a standard deviation of 4.3° in the 30 s test.

The final step is to determine the phase difference $\phi_s(0) - \phi_r(0)$ present in Eqs. (2) and (4). Here we optimize this value based on the least squares method, taking both the detections of strong phase reference and dim phase reference into account. (See Supplemental Material [28] for details of the phase estimation). In the experiment, this phase difference is calculated and refreshed every 500 ms, to avoid any accumulated errors due to inaccurate wavelength settings, high-order residual phase errors, and accumulated errors in estimating strong phase reference.

Result.—Our system runs at a 1 GHz frequency with a signal pulse width of 120 ps. The quantum signals are not sending in the first 400 ns of the 1 μs period when strong phase reference emits, or in the first 40 ms of the 100 ms period when dim phase reference is sending. Further, the detected quantum signals near the edges of these strong light are also dropped, to avoid potential noises. The effective signal frequency is 351 MHz.

The dark counts of the ultralow noise SNSPDs are measured to be 0.014 and 0.026 Hz on installation, with detection efficiencies of 60% and 55%. The total noises of the λ_2 quantum channel is measured to about 0.019 and 0.035 Hz, when the strong phase reference is on. In data processing, we employ a 200 ps window to further filter the noises, whose efficiency is about 65%. We note the SNSPD dark counts increased during the experimental tests.

We take measurements at total fiber distances between 202 and 1002 km between Alice and Bob, from 31.6 to 156.5 dB in a symmetric fiber setup. The secure key rates are summarized in Fig. 3. Positive secure keys are generated in asymptotic regime for the 1002 km case, and in finite size regimes for all other distances.

In the longest distribution distance of 1002 km, a total of 1.02×10^{14} signal pulses are sent. The secure key rate is

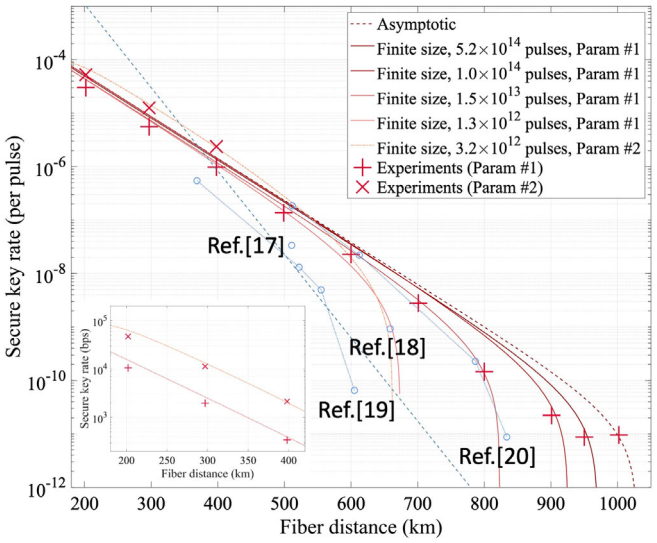

FIG. 3. Simulations and experimental results of the secure key rates. The +-shape points are our experimental results using the parameters optimized for long distance (parameter No. 1), the ×-shape points are our experimental results using the parameters optimized for short distance (parameter No. 2). The solid curves are the simulation results considering the finite size effect. The red dashed curve is the simulation result with infinite size assumption. The circle markers indicates the state-of-the-art TF-QKD results reported in Refs. [17–20]. The blue dashed line shows the PLOB bound. Inset: the secure key rate per second in short distances.

calculated as 9.53×10^{-12}, which is 0.0034 bps, considering the effective signal frequency. We note that due to the narrow linewidth laser used in the experiment, the fiber length between Alice-Charlie and Bob-Charlie do not have to be exactly the same. For example, the fiber distances in this test are 500 and 502 km between Alice-Charlie and Bob-Charlie, respectively.

The finite size effect [27] is taken into consideration for all other experimental tests with the fiber lengths between 202 and 952 km for composable security under any coherent attack [26,27]. In the calculation, the error correction inefficiency is set to $f = 1.16$, the statistics block size is set to the complete length of the test, the failure probability of applying the Chernoff bound in the finite-size estimation is set to $\varepsilon = 10^{-10}$, the failure probability of the error correction process and the privacy amplification process are set to $\varepsilon_{\mathrm{cor}} = \varepsilon_{\mathrm{PA}} = 10^{-10}$, and the coefficient of the chain rules of smooth min and max entropies is set to $\hat{\varepsilon} = 10^{-10}$.

We test the performance for all the fiber distances with the parameters optimized for long distance (the "+" shape points in Fig. 3). The number of signal pulses sent is 5.18×10^{14} in the 952 km case, 1.02×10^{14} in the 901 km case, 1.52×10^{13} in the 600 to 800 km cases, and 1.26×10^{12} in the 202 to 499 km cases. The secure key rate in the 952 km case is calculated as 8.75×10^{-12}, which is 0.0031 bps. (See Supplemental Material [28] for details of parameters and results). The secure key rates exceed the absolute PLOB bound [36] for all the tests with the fiber distances equal to or longer than 398 km, where the PLOB bound is calculated as $-\log_2(1-\eta)$ with the optical and detection efficiency in Charlie set to $\eta_{\mathrm{opt}} = 100\%$.

Next, we optimized the parameters for short distance, and performed the experiment for 202 to 398 km again (the "×" shape points in Fig. 3). The dim phase reference is set to 400 ns in the 1 μs signal period, the intensity set to the quantum signal level through all the 100 ms period. The effective signal frequency is thus increased to 900 MHz. The number of signal pulses sent is 3.24×10^{12} in the same collection time as the previous 202 to 398 km tests. The secure key rate is increased from 3.01×10^{-5} to 5.23×10^{-5} for the 202 km test, with the key rate per second increased from 10.56 to 47.06 kbps.

Conclusion.—In conclusion, we experimentally demonstrated an SNS-TF-QKD over 1002 km in the infinite regime and up to 952 km considering the finite size effect. The main elements enabling the ultralong distance experiment include the ultra-low-loss fiber, the ultra-low-noise SNSPD, and the time-multiplexed dual-band phase stabilization method. Our experiment demonstrates the feasibility of SNS-TF-QKD through the extremely long fiber channel. The secure key rate through shorter fiber is applicable in many practical scenarios. We expect the technology developed in this work will find more general applications in quantum communications [37].

The authors would like to thank W. Li for the help in developing the phase stabilization method, and X.-L. Hu for the help in the secure key rate calculation. This work was supported by the National Key Research and Development (R&D) Plan of China (Grant No. 2020YFA0309800), the National Natural Science Foundation of China (Grants No. T2125010, No. 12174215, No. 61971409 and No. 61971408), the Chinese Academy of Sciences, Key R&D Plan of Shandong Province (Grant No. 2020CXGC010105), Shandong provincial natural science foundation (Grants No. ZR2020YQ45 and No. ZR202209150053). Y. L. and Q. Z. acknowledge support from the Taishan Scholar Program of Shandong Province, W.-J. Z. acknowledges support from the Youth Innovation Promotion Association (No. 2019238).

Y. L. and W.-J. Z. contributed equally to this work.

*lxyou@mail.sim.ac.cn
†xbwang@mail.tsinghua.edu.cn
‡qiangzh@ustc.edu.cn
¶pan@ustc.edu.cn

[1] C. H. Bennett and G. Brassard, in *Proceedings of the IEEE International Conference on Computers, Systems, and Signal Processing* (1984), pp. 175–179.
[2] A. K. Ekert, Phys. Rev. Lett. **67**, 661 (1991).
[3] N. Gisin, G. Ribordy, W. Tittel, and H. Zbinden, Rev. Mod. Phys. **74**, 145 (2002).
[4] V. Scarani, H. Bechmann-Pasquinucci, N. J. Cerf, M. Dušek, N. Lütkenhaus, and M. Peev, Rev. Mod. Phys. **81**, 1301 (2009).
[5] N. Gisin, Front. Phys. **10**, 100307 (2015).
[6] F. Xu, X. Ma, Q. Zhang, H.-K. Lo, and J.-W. Pan, Rev. Mod. Phys. **92**, 025002 (2020).
[7] S. Pirandola, U. L. Andersen, L. Banchi, M. Berta, D. Bunandar, R. Colbeck, D. Englund, T. Gehring, C. Lupo, C. Ottaviani *et al.*, Adv. Opt. Photonics **12**, 1012 (2020).
[8] W. K. Wootters and W. H. Zurek, Nature (London) **299**, 802 (1982).
[9] M. Lucamarini, Z. L. Yuan, J. F. Dynes, and A. J. Shields, Nature (London) **557**, 400 (2018).
[10] M. Minder, M. Pittaluga, G. Roberts, M. Lucamarini, J. Dynes, Z. Yuan, and A. Shields, Nat. Photonics **13**, 334 (2019).
[11] S. Wang, D.-Y. He, Z.-Q. Yin, F.-Y. Lu, C.-H. Cui, W. Chen, Z. Zhou, G.-C. Guo, and Z.-F. Han, Phys. Rev. X **9**, 021046 (2019).
[12] Y. Liu, Z.-W. Yu, W. Zhang, J.-Y. Guan, J.-P. Chen, C. Zhang, X.-L. Hu, H. Li, C. Jiang, J. Lin *et al.*, Phys. Rev. Lett. **123**, 100505 (2019).
[13] X. Zhong, J. Hu, M. Curty, L. Qian, and H.-K. Lo, Phys. Rev. Lett. **123**, 100506 (2019).
[14] X.-T. Fang, P. Zeng, H. Liu, M. Zou, W. Wu, Y.-L. Tang, Y.-J. Sheng, Y. Xiang, W. Zhang, H. Li *et al.*, Nat. Photonics **14**, 422 (2020).

[15] J.-P. Chen, C. Zhang, Y. Liu, C. Jiang, W. Zhang, X.-L. Hu, J.-Y. Guan, Z.-W. Yu, H. Xu, J. Lin *et al.*, Phys. Rev. Lett. **124**, 070501 (2020).
[16] H. Liu, C. Jiang, H.-T. Zhu, M. Zou, Z.-W. Yu, X.-L. Hu, H. Xu, S. Ma, Z. Han, J.-P. Chen *et al.*, Phys. Rev. Lett. **126**, 250502 (2021).
[17] J.-P. Chen, C. Zhang, Y. Liu, C. Jiang, W.-J. Zhang, Z.-Y. Han, S.-Z. Ma, X.-L. Hu, Y.-H. Li, H. Liu *et al.*, Nat. Photonics **15**, 570 (2021).
[18] J.-P. Chen, C. Zhang, Y. Liu, C. Jiang, D.-F. Zhao, W.-J. Zhang, F.-X. Chen, H. Li, L.-X. You, Z. Wang, Y. Chen, X.-B. Wang, Q. Zhang, and J.-W. Pan, Phys. Rev. Lett. **128**, 180502 (2022).
[19] M. Pittaluga, M. Minder, M. Lucamarini, M. Sanzaro, R. I. Woodward, M.-J. Li, Z. Yuan, and A. J. Shields, Nat. Photonics **15**, 530 (2021).
[20] S. Wang, Z.-Q. Yin, D.-Y. He, W. Chen, R.-Q. Wang, P. Ye, Y. Zhou, G.-J. Fan-Yuan, F.-X. Wang, W. Chen, Y.-G. Zhu, P. V. Morozov, A. V. Divochiy, Z. Zhou, G.-C. Guo, and Z.-F. Han, Nat. Photonics **16**, 154 (2022).
[21] X.-B. Wang, Z.-W. Yu, and X.-L. Hu, Phys. Rev. A **98**, 062323 (2018).
[22] X.-L. Hu, C. Jiang, Z.-W. Yu, and X.-B. Wang, Quantum Sci. Technol. **7**, 045031 (2022).
[23] H. Xu, Z.-W. Yu, C. Jiang, X.-L. Hu, and X.-B. Wang, Phys. Rev. A **101**, 042330 (2020).
[24] C. Jiang, X.-L. Hu, H. Xu, Z.-W. Yu, and X.-B. Wang, New J. Phys. **22**, 053048 (2020).
[25] Z.-W. Yu, X.-L. Hu, C. Jiang, H. Xu, and X.-B. Wang, Sci. Rep. **9**, 3080 (2019).
[26] C. Jiang, Z.-W. Yu, X.-L. Hu, and X.-B. Wang, Phys. Rev. Appl. **12**, 024061 (2019).
[27] C. Jiang, X.-L. Hu, Z.-W. Yu, and X.-B. Wang, New J. Phys. **23**, 063038 (2021).
[28] See Supplemental Material at http://link.aps.org/supplemental/10.1103/PhysRevLett.130.210801 for details of the theoretical calculations, the experimental technologies, the parameters, and the experimental results.
[29] H. Chernoff, Ann. Math. Stat. **23**, 493 (1952).
[30] A. Vitanov, F. Dupuis, M. Tomamichel, and R. Renner, IEEE Trans. Inf. Theory **59**, 2603 (2013).
[31] R. V. Pound, Rev. Sci. Instrum. **17**, 490 (1946).
[32] R. Drever, J. L. Hall, F. Kowalski, J. Hough, G. Ford, A. Munley, and H. Ward, Appl. Phys. B **31**, 97 (1983).
[33] C. Clivati, A. Meda, S. Donadello, S. Virzì, M. Genovese, F. Levi, A. Mura, M. Pittaluga, Z. Yuan, A. J. Shields *et al.*, Nat. Commun. **13**, 157 (2022).
[34] W. Zhang, X. Yang, H. Li, L. You, C. Lv, L. Zhang, C. Zhang, X. Liu, Z. Wang, and X. Xie, Supercond. Sci. Technol. **31**, 035012 (2018).
[35] W. Zhang, L. You, H. Li, J. Huang, C. Lv, L. Zhang, X. Liu, J. Wu, Z. Wang, and X. Xie, Sci. China Phys. Mech. Astron. **60**, 120314 (2017).
[36] S. Pirandola, R. Laurenza, C. Ottaviani, and L. Banchi, Nat. Commun. **8**, 15043 (2017).
[37] Y.-A. Chen, Q. Zhang, T.-Y. Chen, W.-Q. Cai, S.-K. Liao, J. Zhang, K. Chen, J. Yin, J.-G. Ren, Z. Chen *et al.*, Nature (London) **589**, 214 (2021).